PERGAMON

International Journal of Heat and Mass Transfer 45 (2002) 4663–4674

International Journal of HEAT and MASS TRANSFER

www.elsevier.com/locate/ijhmt

Simultaneous estimation of extinction coefficient distribution, scattering albedo and phase function of a two-dimensional medium

Nai-Rui Ou, Chih-Yang Wu *

Department of Mechanical Engineering, National Cheng Kung University, Tainan 701, Taiwan, ROC

Received 26 September 2001; received in revised form 20 March 2002

Abstract

In this work, we develop a scheme based on solving the general integro-differential equation of radiation transport to estimate simultaneously the distribution of the extinction coefficient, the scattering albedo and the phase function of a two-dimensional inhomogeneneous medium with less diffusive radiation. The forward problem for a cylindrical medium subjected to collimated incident radiation is solved by the discrete-ordinate method. The inverse radiation problem is formulated as a least square problem that minimizes the discrepancy between the measured and the calculated leaving radiative fluxes. The Levenberg–Marquardt algorithm is applied to the least square problems for a variety of cases. The results obtained show that this scheme can reconstruct accurate enough results for most of the cases considered. Comparisons of the results show that the accuracy of the estimated results decreases with the increase of the scattering albedo and we need more discrete ordinates to generate accurate enough estimated results for an optically thin case. The estimated results obtained from the measurement data with moderate errors are still acceptable.

1. Introduction

Determination of the radiative properties and the source terms of participating media from the available measurements of radiative intensities or fluxes has attracted great attention in many areas, such as optical tomography in medical imaging [1,2], estimating radiative properties of flames and fibrous insulation materials [3–7] and atmosphere remote sensing [8]. While the radiation measurements have the advantage of being non-invasive for the inverse problems of estimating properties, the reliability of the techniques depends on the numerical scheme adopted for inverse problem calculation. Many schemes, such as the transmission tomography [3,4,6,9], developed for non-scattering cases are quite effective and robust. Instead of the transmission tomography, Mengüc and coworkers developed a scattering tomography to determine the radiative properties in radially inhomogeneous sooting flames [5,10]. First two orders of scattering are accounted in their work and the results are in good agreement with theory until an optical thickness of 1.0 [5]. However, radiation transport with high orders of scattering, such as radiative heat transfer in fibrous insulation materials and visible light propagation in biological tissues, makes the application of the above technique difficult, so increasingly attention is turning to iterative, optimization-based reconstruction methods. To solve the forward problem of radiation transport mapping a given solution of absorbing and scattering properties to the corresponding boundary measurements, several approaches have been used by the reconstruction methods [1,2]. Statistical methods, such as Monte Carlo and random walk methods, are employed by many authors [1,2]. However, they are prohibitively costly in computation time and care has to be taken with the statistical error [2]. The diffusion approximation frequently adopted by optical tomography reduces the integro-differential equation of radiation transport to differential equations by expanding the intensity in a

* Corresponding author. Tel.: +886-6-275-7575; fax: +886-6-235-2973.

E-mail address: cywu@mail.ncku.edu.tw (C.-Y. Wu).

0017-9310/02/$ - see front matter
PII: S0017-9310(02)00168-0

Nomenclature

$A_k, \widehat{A}_k$	coefficients of exact and estimated phase functions, respectively, see Eqs. (2) and (9)
a_{mn}, b_{mn}	coefficients of estimated distribution of the extinction coefficient, see Eq. (10)
F	objective function to be minimized, see Eq. (11)
I	dimensionless radiation intensity
I^i	radiation intensity of irradiation at $(1, \psi^i)$ along the propagation direction $(\psi^i + \pi, 0)$, see Fig. 1
K, $\widehat{K}$	orders of the exact and estimated phase function expansions, respectively
$\widehat{M}_\beta$, $\widehat{N}_\beta$, $\widehat{L}_\beta$	orders of expansion in the r-, ψ- and z-directions, respectively, for the estimated distribution of the extinction coefficient, see Eq. (10) and Eq. (13)
N_{ψ_x}, M_θ	numbers of discrete ordinates, see Eq. (8)
N_r, N_ψ, N_z	numbers of cells in the r-, ψ- and z-directions, respectively
N_i	total number of incidence, see Eq. (11)
N_l	number of measured leaving radiative fluxes for each incidence, see Eq. (11)
$\tilde{q}^i$, $\hat{q}^i$	ith measured and estimated dimensionless leaving radiative fluxes, respectively, see Eq. (11)
r	dimensionless radial coordinate
r_0	radius of the cylindrical medium
r_1, r_2	variables defined in Table 1
z	dimensionless axial coordinate
w	quadrature weight

Greek symbols

Φ, $\widehat{\Phi}$	exact and estimated phase functions, respectively
β, $\hat{\beta}$	exact and estimated dimensionless extinction coefficients, respectively
κ	absorption coefficient
η, μ, ξ	direction cosines, see Eq. (1)
θ	polar angle, see Fig. 1
θ_0	angle defined as $\theta_0 = \mu\mu' + \eta\eta' + \xi\xi'$, see Eq. (2)
σ	ratio of the standard deviation of the measurement data to its exact value
σ_s	scattering coefficient
ω, $\hat{\omega}$	exact and estimated albedos, respectively
ψ	spatial azimuthal angle, see Fig. 1
ψ^i	spatial azimuthal angle of the incident point, see Fig. 1
ψ_x	directional azimuthal angle relative to the x-axis, see Fig. 1
ζ	random variable
τ_c	optical path length, see Eq. (5)

Superscripts

c	collimated part
d	diffuse part
i	ith incidence

Subscripts

b	backward direction
f	forward direction
i	index of the r-coordinate, or the ith incidence
j	index of the ψ-coordinate
l	location of leaving radiative flux, or index used in Eq. (13)
m, n	index of discrete ordinates, see Eq. (8), or index used in Eq. (10)
r	radial coordinate
θ	polar angle, see Fig. 1
ψ	spatial azimuthal angle, see Fig. 1
ψ_x	directional azimuthal angle relative to x-axis, see Fig. 1

series of spherical harmonics and by employing an anisotropy parameter to approximate the scattering phase function [1,2]. The diffuse optical tomography is very successful in clinical applications, because most tissues of interest are optically thick and strongly scattering. However, when the optical tomography is applied to imaging of the brain, the domain of interest includes non-diffusive regions [11]. For engineering application, such as estimating radiative properties of flames, the radiation field is not diffusive enough either. Either the direct or the inverse analysis of the less diffusive radiation in an optically not thin medium requires rigorous solution methods. However, only a few researchers used rigorous methods to reconstruct the radiation parameters for multi-dimensional media and only a part of the unknown radiation parameters was estimated simultaneously. Some inverse analysis techniques were reviewed by McCormick [12]. Yuen and co-worker applied a generalized zonal method to estimate the extinction coefficient and the scattering albedo of a two-dimensional medium [7]. Aronson and co-workers used Monte Carlo procedures to simulate the scattering of a laser beam in a tissue slab and determine regions of absorption inhomogeneity [13]. Chang and co-workers applied the Monte Carlo simulations to the recovery of the perturbation changes in absorptions for a cylindrical medium [14]. Klose and Hielscher reconstructed the scattering coefficient of a two-dimensional medium by solving the discrete-ordinate

formulation of the transport forward model in rectangular coordinates [15,16]. There are few works on the inverse analysis of all radiation parameters of multi-dimensional media considering cases with less diffusive radiation, which shall be described by the general integro-differential equation of radiation transport. The less diffusive radiation appears, when the optical size of the medium is not large or the scattering is not strong. Thus, this work aims to develop a scheme based on solving the general integro-differential equation of radiation transport to estimate the distributions of all unknown radiation parameters, including the extinction coefficient, the scattering albedo and the phase function of an inhomogeneous multi-dimensional medium. The effects of various computational and physical parameters, including the order of expansion for distributions of the extinction coefficient and the phase function, the number of discrete ordinates, the numbers of incidences and measured leaving radiative fluxes, the optical size, the scattering albedo, and the measurement error, on the estimated results are examined.

In this work, we consider a complete scattering model, including the high-order expansion of phase function, for a cylindrical medium subjected to collimated incident radiation. The forward problem is solved by a modified discrete-ordinate method (DOM), which can remedy the ray effects [17,18]. The inverse radiation is formulated as a least square problem that minimize the discrepancy between the measured and the calculated leaving radiative fluxes. A standard least-square optimization procedure, the Levenberg–Marquardt algorithm, is used to solve the inverse problem. The inverse scheme based on transport calculations solving the exact formulation of radiative transfer is applied to a variety of cases, including those with less diffusive radiation. The scheme is mainly applied to two-dimensional inhomogeneous media; for the purpose of comparison, we also consider a three-dimensional case.

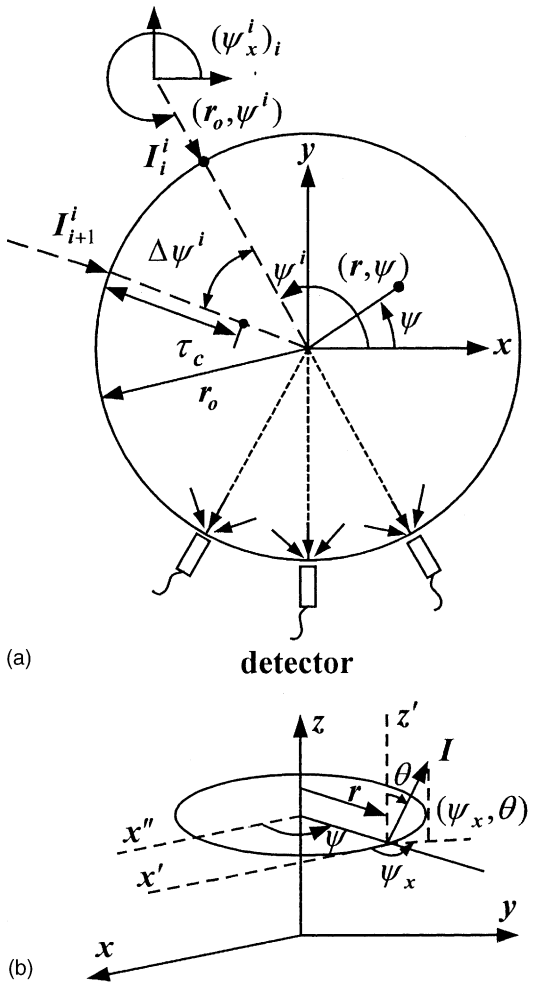

Fig. 1. Physical model and coordinates: (a) physical model, (b) coordinates.

2. Analysis

In this section we aim to develop a scheme to estimate the unknown radiative properties of a participating medium by utilizing the measured fluxes leaving the medium, as shown in Fig. 1(a). First, we consider radiative transfer in an absorbing and scattering cylindrical medium with a transparent boundary. The emission of the medium is far less than the incident radiation, and so the emission is negligible in the present analysis. When the incident radiations do not vary along the axial direction, the medium extends to infinity in the axial direction, and the absorption and scattering coefficients of the medium (κ and σ_s) may vary only radially and azimuthally, the problem is two-dimensional. Otherwise, either the forward problem of the inverse problem is three-dimensional. The following is the two-dimensional version of the problem. The position in the radiative field can be specified by the azimuthal angle ψ and the dimensionless coordinate r defined as the radial geometrical variable divided by the radius r_0. The propagation direction of the radiation intensity at that point can be specified by (ψ_x,θ), where either ψ_x or θ is defined by the angle between the propagation direction of radiation and a Cartesian coordinate, as shown in Fig. 1(b). Thus a set of fixed values (ψ_x,θ) defines the same propagation direction at any spatial location. The transport equation of radiative transfer can be expressed as

$$\mu\frac{\partial}{\partial r}I(r,\psi,\psi_x,\xi)+\frac{\eta}{r}\frac{\partial}{\partial\psi}I(r,\psi,\psi_x,\xi)+\beta(r,\psi)I(r,\psi,\psi_x,\xi)$$
$$=\frac{\omega(r,\psi)\beta(r,\psi)}{4\pi}\int_{\psi_x'=0}^{2\pi}\int_{\xi'=-1}^{1}I(r,\psi,\psi_x',\xi')$$
$$\times\Phi(r,\psi,\psi_x,\xi,\psi_x',\xi')\mathrm{d}\xi'd\psi_x' \quad 0\leqslant r\leqslant 1,\ 0\leqslant\psi<2\pi,$$
$$0\leqslant\psi_x<2\pi,\ -1\leqslant\xi\leqslant 1, \tag{1}$$

where μ denotes the directional cosine defined as $\mu = \sin\theta\cos(\psi_x - \psi)$, $I(r,\psi,\psi_x,\xi)$ the radiation intensity non-dimensionalized by the irradiation intensity I^i at $r = 1$ and $\psi = \psi^i$ along the direction defined by $\mu = -1$ and $\xi = 0$, ξ the directional cosine defined as $\xi = \cos\theta$, η the directional cosine defined as $\eta = \sin\theta \times \sin(\psi_x - \psi)$, β the dimensionless extinction coefficient defined as $(\kappa + \sigma_s)r_0$, ω the scattering albedo defined as $\sigma_s/(\kappa + \sigma_s)$, and Φ the scattering phase function expressed in the form

$$\Phi(r,\psi,\psi_x,\xi,\psi'_x,\xi') = \sum_{k=0}^{K} A_k(r,\psi)P_k(\cos\theta_0). \tag{2}$$

Here, K denotes the order of anisotropic scattering, A_k the coefficient of the expansion with $A_0 = 1$, P_k the kth-order Legendre polynominal, and $\theta_0 = \cos^{-1}(\mu\mu' + \eta\eta' + \xi\xi')$. The dimensionless boundary condition for this problem can be expressed as

$$I(1,\psi,\psi_x,\xi) = \begin{cases} 1 & \text{at } \psi = \psi^i, \mu = -1, \xi = 0, \\ 0 & \text{otherwise,} \end{cases}$$
$$0 \leqslant \psi < 2\pi, \quad -1 \leqslant \xi \leqslant 1, \quad \pi/2 \leqslant (\psi_x - \psi) \leqslant 3\pi/2. \tag{3}$$

Next, we adopt a modified DOM [17,18] to solve the forward problem of radiation transport. When the optical thickness is small and radiative property distribution or the incident radiation from the boundary has abrupt variation, the ordinary DOM may suffer from the ray effects. Thus, similarly to the modified DOM used by Liou and Wu [17] and Ramankutty and Crosbie [18], we decompose I into the fairly diffuse part I^d and the collimated part I^c. The latter is zero except that

$$I^c(r,\psi,\psi^i + \pi, 0) = e^{-\tau_c(r,\psi)} \quad \text{for } \psi = \psi^i \text{ or } \psi = \psi^i + \pi \tag{4}$$

with

$$\tau_c(r,\psi) = \begin{cases} \int_r^1 \beta(r',\psi^i)\,dr' \\ \quad \text{for } \psi = \psi^i \\ \int_0^1 \beta(r',\psi^i)\,dr' + \int_0^r \beta(r',\psi^i + \pi)\,dr' \\ \quad \text{for } \psi = \psi^i + \pi \end{cases} \tag{5}$$

Substituting Eqs. (4) and (5) into Eq. (1) yield the transport equation for I^d as

$$\mu\frac{\partial}{\partial r}I^d(r,\psi,\psi_x,\xi) + \frac{\eta}{r}\frac{\partial}{\partial\psi}I^d(r,\psi,\psi_x,\xi) + \beta(r)I^d(r,\psi,\psi_x,\xi)$$
$$= \frac{\omega(r,\psi)\beta(r,\psi)}{4\pi}\int_{-1}^{1}\int_0^{2\pi} I^d(r,\psi,\psi'_x,\xi') \times \Phi(r,\psi,\psi_x,\xi,\psi'_x,\xi')\,d\psi'_x\,d\xi' + \frac{\omega(r,\psi)\beta(r,\psi)}{4\pi} \times \Phi(r,\psi,\psi_x,\xi,\psi^i + \pi, 0)I^c(r,\psi,\psi^i + \pi, 0),$$
$$0 \leqslant r \leqslant 1, \quad 0 \leqslant \psi < 2\pi, \quad 0 \leqslant \psi_x < 2\pi, \quad -1 \leqslant \xi \leqslant 1, \tag{6}$$

The boundary condition for I^d is

$$I^d(1,\psi,\psi_x,\xi) = 0 \quad 0 \leqslant \psi < 2\pi, \quad -1 \leqslant \xi \leqslant 1, \quad \pi/2 \leqslant (\psi_x - \psi) \leqslant 3\pi/2. \tag{7}$$

While Eq. (4) is the exact solution of I_c, we adopt a DOM scheme [19] to solve $I^d(r,\psi,\psi_x,\xi)$.

The discrete-ordinate approximation of Eq. (6) can be expressed as:

$$\mu_{n,m}(\psi)\frac{\partial}{\partial r}I^d_{n,m}(r,\psi) + \frac{\eta_{n,m}(\psi)}{r}\frac{\partial}{\partial\psi}I^d_{n,m}(r,\psi) + \beta(r,\psi)I^d_{n,m}(r,\psi)$$
$$= \frac{\omega(r,\psi)\beta(r,\psi)}{4\pi}\left\{\left[\sum_{n'=1}^{N_{\psi_x}}\sum_{m'=1}^{M_\theta} I^d_{n',m'}(r,\psi)\Phi_{n,m,n',m'}(r,\psi)w_{n',m'}\right] + \Phi_{n,m,n^i,m^i}(r,\psi)I^c_{n^i,m^i}(r,\psi)\right\} \quad \text{for } 0 \leqslant r \leqslant 1, \ 0 \leqslant \psi < 2\pi,$$
$$n = 1,2,\ldots,N_{\psi_x}, \ m = 1,2,\ldots,M_\theta \tag{8}$$

where the subscripts n and m represent the discrete directions, $w_{n',m'}$ the quadrature weight, the subscripts n^i, m^i the direction of incident radiation, N_{ψ_x} and M_θ the numbers of discrete ordinates over $0 \leqslant \psi_x \leqslant 2\pi$ and $-\pi/2 \leqslant \theta \leqslant \pi/2$, respectively. We divide the whole domain into $N_r \times N_\psi$ cells, where N_r and N_ψ denote the numbers of cells in the r and ψ directions, respectively. By the same procedure as Ref. [19], we can obtain the finite-difference approximation of Eq. (8), and the resulting algebraic equations are solved by Gauss–Seidel method. Therefore, by giving the relevant absorbing and scattering properties, we can get the corresponding leaving radiative fluxes.

To solve the inverse problem, we consider radiative transfer in a medium composed of same species of particles with variable concentration. The radiative properties of such a medium can be described by a variable extinction coefficient, a constant scattering albedo and a constant phase function. Moreover, the particles are assumed to be perfect spherical, and so the phase function is independent of azimuthal angle and only concerned with the angle formed by the direction of incident ray and the forward direction of the scattered ray (θ_0). Thus, the unknown phase function is expressed as

$$\hat{\Phi} = \sum_{k=0}^{\widehat{K}} \widehat{A}_k P_k(\cos\theta_0) \tag{9}$$

and the unknown albedo is denoted by $\hat{\omega}$. The unknown distribution of the extinction coefficient is expressed as

$$\hat{\beta}(r,\psi) = a_{00} + \sum_{m=1}^{\widehat{M}_\beta}\sum_{n=0}^{\widehat{N}_\beta} r^m[a_{mn}\cos(n\psi) + b_{mn}\sin(n\psi)], \quad 0 \leqslant r \leqslant 1, \ 0 \leqslant \psi < 2\pi. \tag{10}$$

Now, to reconstruct the radiative properties of the medium is equivalent to find $\hat{\omega}$, $\widehat{A}_k$, a_{mn} and b_{mn}. Here, we

try to find those unknowns by minimizing the objective function

$$F=\sum_{i=1}^{N_i}\sum_{l=1}^{N_l}\left\{\tilde{q}^i_{N_r+1/2,l}-\hat{q}^i_{N_r+1/2,l}\left[\hat{\beta}(r,\psi),\hat{\omega},\widehat{\Phi}\right]\right\}^2, \quad (11)$$

where i denotes the ith incidence, N_i the total number of incidences, l the lth measured point under the ith incidence, N_l the total number of measured leaving radiative fluxes for each incidence, $\tilde{q}^i_{N_r+1/2,l}$ and $\hat{q}^i_{N_r+1/2,l}$ the measured and estimated leaving radiative fluxes in the radial direction at the boundary $r=1$, respectively. By N_i times of incidences and N_l measured data generated for each incidence, $N_i\times N_l$ measured data can be obtained to reconstruct the radiative properties. To determine those unknowns, the number of the measured data $(N_i\times N_l)$ shall be greater than the number of unknowns, $2\times[\widehat{M}_\beta\times(\widehat{N}_\beta+1)]+\widehat{K}+2$.

As shown in Fig. 1(a), the incident radiation enters the domain considered once at only one location of the peripheral cylindrical surface surrounding the medium and the radiative fluxes leaving the peripheral cylindrical surface are measured at the other N_l locations. We consider those locations to be equally spaced by the azimuthal angle $\Delta\psi=2\pi/N_i$. While the incident radiation enters the domain at a different location, we measure the other set of the leaving radiative fluxes. The leaving radiative flux caused by the ith incidence could be expressed as:

$$q^i_{N_r+1/2,j}=\left\{\begin{array}{ll}\sum_{n=1}^{N_{\psi_x}}\sum_{m=1}^{M_\theta} I_{N_r+1/2,j,n,m}\mu_{j,n,m}w_{n,m}+I^{c}_{N_r+1/2,j^i,n^i,m^i}, & j=j^i+N_\psi/2\\ \sum_{n=1}^{N_{\psi_x}}\sum_{m=1}^{M_\theta} I_{N_r+1/2,j,n,m}\mu_{j,n,m}w_{n,m}, & j\neq j^i+N_\psi/2\end{array}\right\}^i \quad \text{for } \mu_{j,n,m}>0. \quad (12)$$

If the distributions of the radiation properties are three-dimensional, we have to solve a three-dimensional problem in terms of the radiation intensity $I(r,\psi,z,\psi_x,\xi)$, which depends on three spatial variables and two directional variables, instead of $I(r,\psi,\psi_x,\xi)$. Besides, one more differential term, $\xi(\partial/\partial z)I(r,\psi,z,\psi_x,\xi)$, shall be added to the governing equation, Eq. (1). To reconstruct the three-dimensional distributions of the radiation properties, we need more data of the leaving fluxes. They can be obtained by scanning the incident beam both along the peripheral and the axial directions over the cylindrical medium. However, the numerical procedure is similar to the two-dimensional one, except that the unknown distribution of the extinction coefficient is expressed as

$$\hat{\beta}(r,\psi,z)=a_{000}+\sum_{m=1}^{\widehat{M}_\beta}\sum_{n=0}^{\widehat{N}_\beta}\sum_{l=1}^{\widehat{L}_\beta} r^m[a_{mnl}\cos(n\psi)+b_{mnl}\sin(n\psi)]z^l+\sum_{m=1}^{\widehat{M}_\beta}a_{m00}r^m+\sum_{l=1}^{\widehat{L}_\beta}a_{00l}z^l \quad (13)$$

The steps of reconstructing radiative properties are summarized as follows:

1. Guess the properties $\hat{\beta}$, $\hat{\omega}$ and $\widehat{\Phi}$ by giving parameters $a_{mn}=0$, $b_{mn}=0$, $\hat{\omega}=0.1$ and $\widehat{A}_k=0$, except that $a_{00}=1$ and $\widehat{A}_0=1$.
2. Solve the forward problem and obtain $\hat{q}^i_{N_r+1/2,j}(\hat{\beta},\hat{\omega},\widehat{\Phi})$ by the DOM.
3. Find the new estimation of parameters a_{mn}, b_{mn}, $\hat{\omega}$ and $\widehat{A}_k$ by minimizing the objective function. A standard least-square optimization procedure, the Levenberg-Marquardt algorithm [20,21], is used here.
4. Stop the iteration, if the two successive estimated values of a_{mn}, b_{mn}, $\hat{\omega}$ and $\widehat{A}_k$ meet one of the following specified criterions. Otherwise return to step 2 with the newest set of estimated parameters.

The stopping criterions are as follows: (i) on two successive iterations each of the parameters agrees to six digits, (ii) on two successive iterations the relative difference of the objective functions is less than 10^{-8}, (iii) the Euclidean norm of the approximate gradient of the objective function is less than 10^{-8}.

3. Results and discussion

To examine the effects of the numbers of the cells and the discrete ordinates, the extinction coefficient with a non-smooth distribution (β_1 listed in Table 1) is considered first. Fig. 2(a) show that the results for 80×96 and 40×48 cells are in excellent agreement, and the results obtained by using 20×24 cells are not accurate enough for this non-smooth extinction coefficient. Fig. 2(b) shows that convergent results can be obtained by using 12×5 discrete ordinates. When the distribution of the extinction coefficient is smooth, the convergent results can be obtained by using less cells and discrete ordinates, as shown in Fig. 3(a). The inverse calculations are carried out to estimate the albedo and the extinction coefficient of the medium with a known phase function for a sequence of M_β's. As shown in Fig. 3(b), the estimated β_2's for ω_1 and ω_3 are in excellent agreement with the exact $\beta'_2 s$ except those obtained by using $\hat{\beta}_2$ with $\widehat{M}_\beta=3$. The recovered value of the albedo is the same as the exact value, except that $\hat{\omega}_3=0.985$ for the calculation with $\widehat{M}_\beta=3$. The comparison reveals that the reconstruction of radiative properties of a highly scattering medium needs high-order expansions of the estimated properties. For the case shown in Fig. 3(b), the

Table 1
Properties of the media considered

Extinction coefficients

$$\beta_1(r)=\begin{cases}1.0 & r\leqslant 0.7\\ 1+5(r-0.7) & 0.7\leqslant r\leqslant 0.75\\ 1.25 & \text{for}\quad 0.75\leqslant r\leqslant 0.8\\ 1.25-10(r-0.8) & 0.8\leqslant r\leqslant 0.85\\ 0.75 & r\geqslant 0.85\end{cases}$$

$$\beta_2(r)=\frac{480}{343}\left(\frac{1}{2}+\frac{11}{8}r^2+\frac{21}{8}r^3-\frac{9}{2}r^4\right)$$

$$\beta_3(r,\psi)=\begin{cases}\dfrac{1125}{128}\left(\dfrac{32}{125}-\dfrac{6}{5}r_1^2+r_1^3\right)+\dfrac{1}{10} & \text{for}\quad r_1\leqslant 0.8\\ \dfrac{1}{10} & r_1>0.8\end{cases}$$

$$\beta_4(r,\psi)=\begin{cases}\dfrac{1125}{128}\left(\dfrac{32}{125}-\dfrac{6}{5}r_2^2+r_2^3\right)+\dfrac{1}{10} & \text{for}\quad r_2\leqslant 0.8\\ \dfrac{1}{10} & r_2>0.8\end{cases}$$

with

$$r_1=\sqrt{[r\cos(\psi)-\tfrac{1}{5}]^2+[\tfrac{5}{4}r\sin(\psi)]^2},$$
$$r_2=\sqrt{[r\cos(\psi)-\tfrac{1}{5}]^2+[r\sin(\psi)]^2}$$

Scattering phase functions

$$\begin{aligned}\Phi_{\mathrm{f}}=1.0&+1.98398P_1(\cos\theta_0)+1.50823P_2(\cos\theta_0)\\&+0.70075P_3(\cos\theta_0)+0.23489P_4(\cos\theta_0)\\&+0.05133P_5(\cos\theta_0)+0.00760P_6(\cos\theta_0)\\&+0.00048P_7(\cos\theta_0)\end{aligned}$$

$$\begin{aligned}\Phi_{\mathrm{b}}=1.0&-0.56524P_1(\cos\theta_0)+0.29783P_2(\cos\theta_0)\\&+0.08571P_3(\cos\theta_0)+0.01003P_4(\cos\theta_0)\\&+0.00063P_5(\cos\theta_0)\end{aligned}$$

with
$\theta_0=\cos^{-1}(\eta\eta'+\eta\eta'+\xi\xi')$

Scattering albedoes
$\omega_1=0.1$
$\omega_2=0.5$
$\omega_3=0.99$

CPU times at $\omega=0.99$ for the calculations using $\hat{\beta}_2$ with $\widehat{M}_\beta=6$, 5, 4 and 3 are 588, 471, 355 and 420 s on IBM Deck 8400, respectively. This is because the $\hat{\beta}_2$ with a too small number of expansion terms ($\widehat{M}_\beta=3$) is a poor estimation of β_2, and so the inverse calculation with $\widehat{M}_\beta=3$ needs a large number of iterations and more CPU time to obtain convergent results. Moreover, the

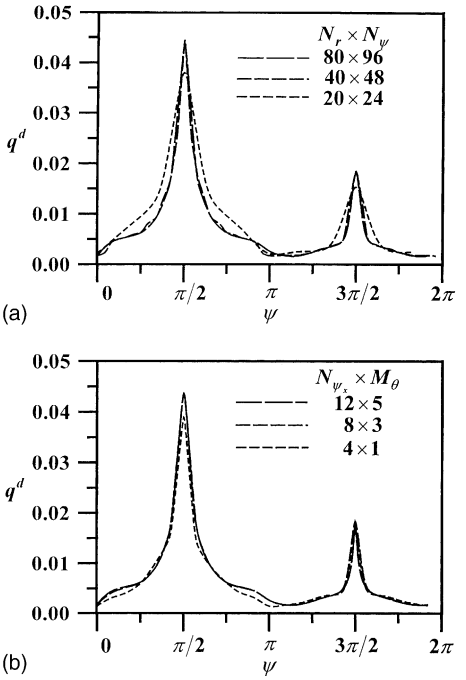

Fig. 2. Distributions of the leaving diffuse radiative fluxes with $\beta=\beta_1$, $\Phi=1.0$ and $\omega=0.5$: (a) different sets of cells, (b) different sets of discrete ordinates.

inverse calculations are carried out to estimate the distribution of a non-smooth extinction coefficient ($\hat{\beta}_1$) for a sequence of M_β's. The convergent results obtained for the extinction coefficient are shown in Fig. 4. It is seen from Fig. 4(a) that the estimated distribution could fit into the convex part of the exact distribution for $\widehat{M}_\beta$ higher up to 12. The estimated distributions for $N_r=80$ seem closer to exact distribution than those for $N_r=40$, as shown in Fig. 4(b). As expected, for the non-smooth β_1, both more cells and higher-order expansions of $\hat{\beta}_1$ are necessary for the accurate estimations of the extinction coefficient. That is, the spatial resolution of the reconstructed results can be improved by using more cells and higher-order expansions of the unknown.

To further examine the effectiveness of the inverse scheme presented above, we consider the reconstruction of more combinations of the distributions of the extinction coefficient, the albedos and the phase functions listed in Table 1. The extinction coefficients are chosen so that the characteristic optical sizes of the media are unity. Here, the characteristic optical size is the optical radius for one-dimensional cases and the optical thickness along x-axis for multi-dimensional cases. Besides, the scattering albedo considered in this work is usually not large ($\omega=0.5$), and so the radiation in those cases is less diffusive. Multiplying a constant to the coefficients

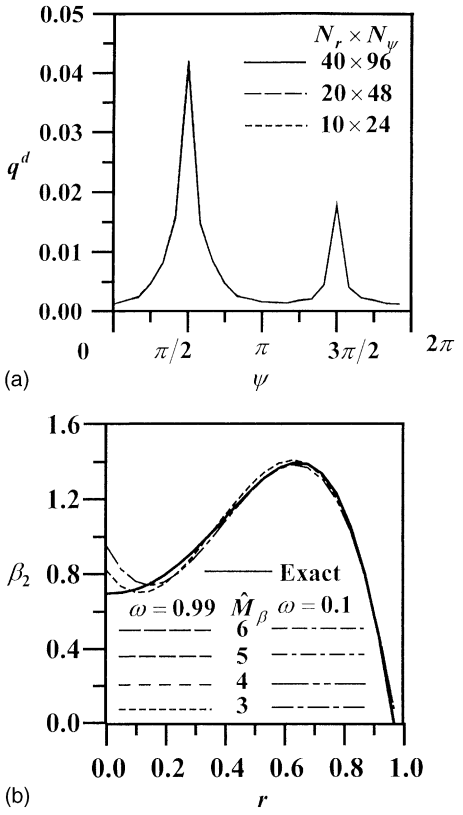

Fig. 3. (a) Distributions of the leaving diffuse radiative fluxes with $\beta = \beta_2$, $\Phi = \Phi_f$ and $\omega = 0.5$, (b) effects of the number of expansion terms of $\hat{\beta}$ for cases with $\omega = 0.1$ and 0.99.

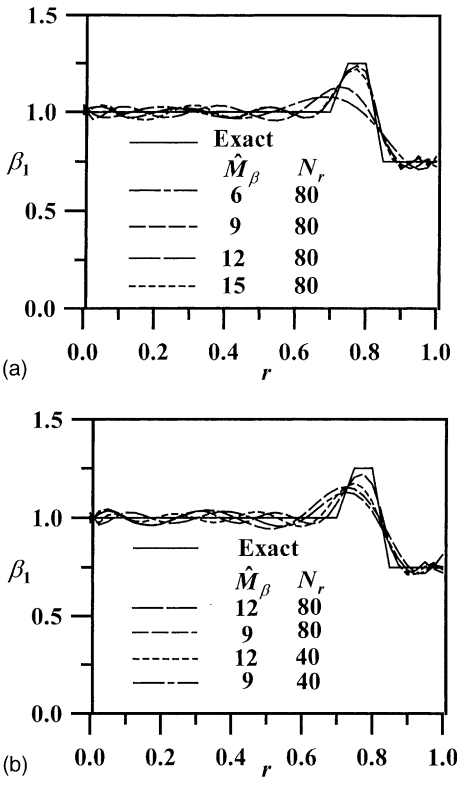

Fig. 4. (a) Effects of the numbers of expansion terms of $\hat{\beta}$ for cases with $\beta = \beta_1$, $\Phi = 1$ and $\omega = 0.5$, (b) two sets of different combined cells and expansion terms.

of β_1, β_2, β_3 or β_4, we can change the characteristic optical size of the medium considered. Performing the forward computations for most of the cases with smooth radiation parameters, we solve the radiative transfer equation along $N_{\psi_x} \times M_\theta = 12 \times 5$ discrete ordinates and divide the domain into $N_r \times N_\psi = 10 \times 24$ cells, except the cases demonstrating the effects of the optical thickness and number of the discrete directions ($N_{\psi_x} \times M_\theta$) on the reconstruction of radiative properties.

To estimate the two-dimensional distribution of the extinction coefficient, we consider the case with $\beta = \beta_3$, $\omega = \omega_2$ and $\Phi = \Phi_b$. The distribution of the extinction coefficient and the albedo are estimated from the knowledge of $N_i \times N_l = 23 \times 23$ leaving radiative fluxes. The exact and estimated distributions of the extinction coefficient along the x- and the y-axis for three sets of $\widehat{M}_\beta \times \widehat{N}_\beta$ are shown in Fig. 5(a) and (b), respectively. The results obtained by using $\hat{\beta}_3$ with $\widehat{M}_\beta \times \widehat{N}_\beta = 5 \times 3$ are in good agreement with the exact distribution of the extinction coefficient. The $\hat{\omega}$ obtained by using $\hat{\beta}_3$ with $\widehat{M}_\beta \times \widehat{N}_\beta = 5 \times 3$ is 0.5, and 0.489, 0.485 for the other two sets of $\widehat{M}_\beta \times \widehat{N}_\beta$. Fig. 6(a) and (b) are the exact distribution (β_3) and the recovered distribution ($\hat{\beta}_3$), respectively, obtained by using $\widehat{M}_\beta \times \widehat{N}_\beta = 5 \times 3$ expansion; they show an overall good agreement. Because of the good agreement of the above results, we adopted $\widehat{M}_\beta = 5$ in the r-direction and $\widehat{N}_\beta = 3$ in the ψ-direction in the following cases.

Fig. 7 shows that the recovered distributions of the extinction coefficient approach the exact distribution as N_i and N_l increase. In this test case, we choose $\Phi = 1$ and $\omega = \omega_2$, and use various combinations of N_i and N_l to reconstruct the distribution of the β_4. The incidence locations are equally spaced by $\Delta\psi = 2\pi/N_i$ around the peripheral cylindrical surface of the medium. The measurement locations are equally spaced by $\Delta\psi = 2\pi/N_i$ for $N_i \times N_l = 24 \times 23$ and 12×11 and by $\Delta\psi = 4\pi/N_i$ for $N_i \times N_l = 24 \times 11$. The estimated distribution of the extinction coefficient obtained from the knowledge of $N_i \times N_l = 24 \times 23$ measurement data shows good agreement with the exact distribution. Thus, we adopt $N_i \times N_l = 1 \times 23$ measurement data for $\beta = \beta_2$ and $N_i \times N_l = 24 \times 23$ measurement data for $\beta = \beta_3$ and $\beta = \beta_4$ in the following cases considered.

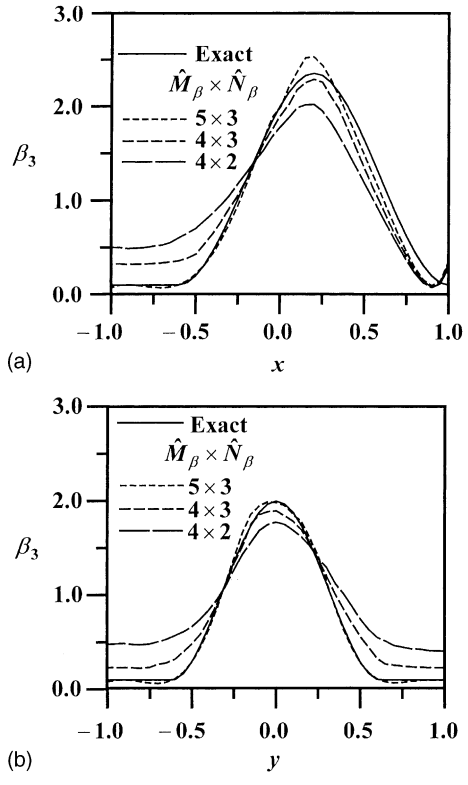

Fig. 5. Effects of the number of expansion terms of $\hat{\beta}$ for the case with $\beta = \beta_3$, $\Phi = \Phi_b$ and $\omega = 0.5$: distributions of the β along (a) the x-axis, (b) y-axis.

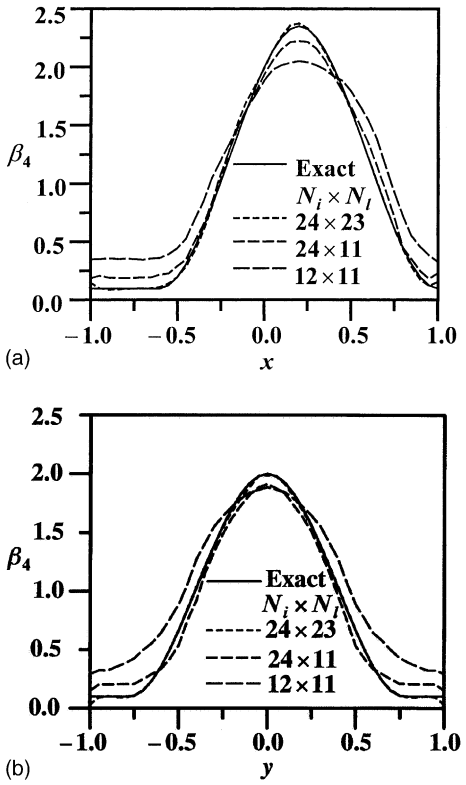

Fig. 7. Effects of the numbers of incidences and measured leaving radiative fluxes for the case with $\beta = \beta_4$, $\Phi = 1.0$ and $\omega = 0.5$: distributions of the β along (a) the x-axis, (b) y-axis.

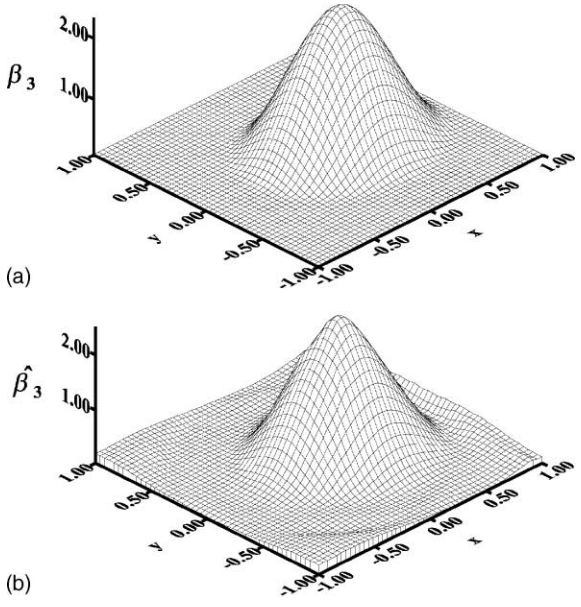

Fig. 6. Two-dimensional distributions of exact and estimated extinction coefficients for the case with $\beta = \beta_3$, $\Phi = \Phi_b$ and $\omega = 0.5$: (a) exact, (b) $\hat{M}_\beta \times \hat{N}_\beta = 5 \times 3$.

By examining the estimated results of the extinction coefficients for the cases with $\Phi = 1$, $\omega = \omega_2$, $\beta = 0.1 \times \beta_4$ and $\beta = 10 \times \beta_4$, we investigate the effects of the optical thickness and the discrete ordinates. The optical thickness along the x-axis is 0.2 for the results shown in Fig. 8(a) and 20 for those shown in Fig. 8(b). When the number of the discrete ordinates (N_{ψ_x} and M_θ) decreases, the outcome of the optically thin case is worse than that of the optically thick case, as shown in Fig. 8(a) and (b). This is because we need more discrete ordinates to obtain accurate solutions of the forward problem for an optically thin case. The comparisons reveal that the number of discrete ordinates has stronger influence on recovering the extinction coefficients for optically thin cases. When dealing with the cases with $\beta = 0.1 \times \beta_4$ and $\beta = 10 \times \beta_4$, we divide the entire domain into $N_r \times N_\psi = 10 \times 24$ and $N_r \times N_\psi = 100 \times 96$ cells, respectively. The CPU time for the optically thick case with $N_{\psi_x} \times M_\theta = 4 \times 1$ is 18,985 s and that for the optically thin case with $N_{\psi_x} \times M_\theta = 4 \times 1$ is 9542 s. The CPU time for the optically thin case with $N_{\psi_x} \times M_\theta = 12 \times 5$, 8×3 and 4×1 are 49,523, 18,247 and 9542 sec on IBM Deck 8400, respectively. Those results of numerical experi-

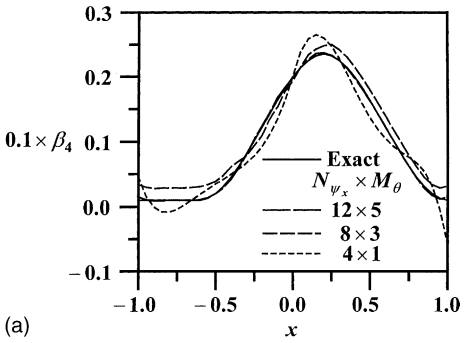

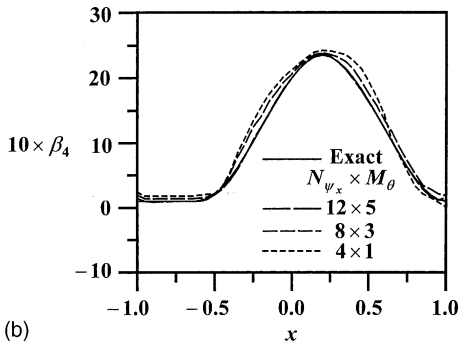

Fig. 8. Effects of the optical size and the number of discrete ordinates for cases with $\Phi = 1.0$, $\omega = 0.5$ and (a) $\beta = 0.1 \times \beta_4$, (b) $\beta = 10 \times \beta_4$.

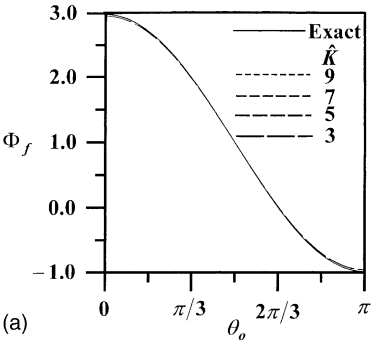

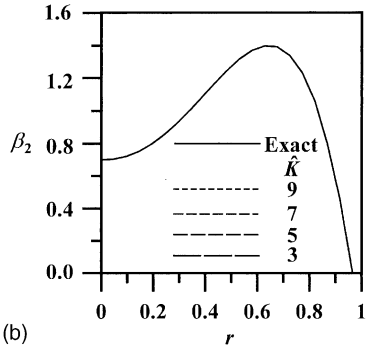

Fig. 9. Effects of the number of anisotropic scattering coefficients for the case with $\beta = \beta_2$, $\Phi = \Phi_f$ and $\omega = 0.5$: (a) distributions of the Φ, (b) distributions of the β.

Table 2
Estimated results ($\hat{\beta}_2$, $\hat{\Phi}_f$ and $\hat{\omega}$) for various scattering albedos and measurement errors (σ)

	σ	$\hat{\omega}$	E_{rms} of $\hat{\beta}_2$	Coefficients of Φ_f
$\omega = \omega_1$	10^{-2}	0.095	2.441%	$\hat{A}_1 = 1.9782$, $\hat{A}_2 = 1.5213$, $\hat{A}_3 = 0.6111$, $\hat{A}_4 = 0.2192$, $\hat{A}_5 = -0.1076$, $\hat{A}_6 = -0.0124$, $\hat{A}_7 = 0.0201$
	10^{-3}	0.098	0.187%	$\hat{A}_1 = 1.9837$, $\hat{A}_2 = 1.5116$, $\hat{A}_3 = 0.6951$, $\hat{A}_4 = 0.2213$, $\hat{A}_5 = 0.0453$, $\hat{A}_6 = 0.0065$, $\hat{A}_7 = 0.0011$
	0	0.1	0.021%	$\hat{A}_1 = 1.9840$, $\hat{A}_2 = 1.5082$, $\hat{A}_3 = 0.7010$, $\hat{A}_4 = 0.2350$, $\hat{A}_5 = 0.0513$, $\hat{A}_6 = 0.0076$, $\hat{A}_7 = 0.0005$
$\omega = \omega_2$	10^{-2}	0.484	3.441%	$\hat{A}_1 = 1.9801$, $\hat{A}_2 = 1.5514$, $\hat{A}_3 = 0.5912$, $\hat{A}_4 = 0.2161$, $\hat{A}_5 = -0.3173$, $\hat{A}_6 = -0.1042$, $\hat{A}_7 = 0.1502$
	10^{-3}	0.495	0.297%	$\hat{A}_1 = 1.9830$, $\hat{A}_2 = 1.5123$, $\hat{A}_3 = 0.6954$, $\hat{A}_4 = 0.2293$, $\hat{A}_5 = 0.0235$, $\hat{A}_6 = -0.0072$, $\hat{A}_7 = 0.0071$
	0	0.500	0.038%	$\hat{A}_1 = 1.9840$, $\hat{A}_2 = 1.5082$, $\hat{A}_3 = 1.7010$, $\hat{A}_4 = 0.2350$, $\hat{A}_5 = 0.0513$, $\hat{A}_6 = 0.0076$, $\hat{A}_7 = 0.0005$
$\omega = \omega_3$	10^{-2}	0.924	8.672%	$\hat{A}_1 = 1.8547$, $\hat{A}_2 = 1.6014$, $\hat{A}_3 = 0.6341$, $\hat{A}_4 = 0.2032$, $\hat{A}_5 = -0.3462$, $\hat{A}_6 = -0.1322$, $\hat{A}_7 = 0.1631$
	10^{-3}	0.959	3.514%	$\hat{A}_1 = 1.9824$, $\hat{A}_2 = 1.5311$, $\hat{A}_3 = 0.7142$, $\hat{A}_4 = 0.2113$, $\hat{A}_5 = 0.0576$, $\hat{A}_6 = -0.0112$, $\hat{A}_7 = 0.0091$
	0	0.989	1.451%	$\hat{A}_1 = 1.9841$, $\hat{A}_2 = 1.5083$, $\hat{A}_3 = 0.7012$, $\hat{A}_4 = 0.2354$, $\hat{A}_5 = 0.0513$, $\hat{A}_6 = 0.0080$, $\hat{A}_7 = 0.0002$

ments show that the CPU times increase with the increase of $N_r \times N_\psi$ and $N_{\psi_x} \times M_\theta$.

Next, we consider complete inverse problems, in which Φ, β, and ω are estimated simultaneously. To

examine the effects of the number of coefficients used in the estimation of the anisotropic phase function, we consider the case with $\Phi = \Phi_f$, $\beta = \beta_2$, and $\omega = \omega_2$. The results shown in Fig. 9(a) and (b) are obtained by using four numbers of anisotropic scattering coefficients, $\widehat{K} = 9$, 7, 5 and 3. As shown in Fig. 9(a) and (b), both sets of curves for the estimated phase function and distributions of the extinction coefficient are in good agreement with the exact Φ and distributions of the β, respectively. The recovered values of $\hat{\omega}$ is 0.5, 0.5, 0.5 and 0.497 for $\widehat{K} = 9$, 7, 5 and 3, respectively. From the above results, it is seen that the number of coefficients of $\widehat{\Phi}$ does not have strong influence on recovering relevant parameters. However, the CPU times for the calculations using $\widehat{\Phi}'s$ with $\widehat{K} = 9$, 7, 5 and 3 are 11100, 3193, 2689 and 4605 s on IBM Deck 8400, respectively. This is because the $\widehat{\Phi}$ with a too small number of expansion terms ($\widehat{K} = 3$) is a poor guess of Φ_f, and so the inverse calculation with $\widehat{K} = 3$ needs a large number of iterations and more CPU time to obtain convergent results.

Since measured data are always accompanied by some errors, the effects of measurement errors on the accuracy of the estimation are also investigated. The simulated measured leaving radiative fluxes with errors ($\tilde{q}^i$) are obtained by adding normal distributed errors to the leaving radiative fluxes (q^i_{exact}) obtained by solving the forward problem with a high-order ($N_{\psi_x} \times M_\theta = 12 \times 5$) scheme and given exact β, ω and Φ. That is,

$$\tilde{q}^i = q^i_{\text{exact}}(1 + \sigma\varsigma), \tag{14}$$

σ is the ratio of the standard deviation of the measurement data to its exact value, and ς is a normal distributed random variable with zero mean and unit standard deviation.

For the sake of comparison, the root mean square error of the estimation of the extinction coefficient is defined as

$$E_{\text{rms}}(\hat{\beta}) = \left\{ \frac{1}{N_r N_\psi} \sum_{i=1}^{N_r} \sum_{j=1}^{N_\psi} \left[\beta(r,\psi) - \hat{\beta}(r,\psi) \right]^2 \right\}^{1/2}. \tag{15}$$

The results of the cases with $\Phi = \Phi_f$, $\beta = \beta_2$ and three different values of ω are listed in Table 2 in terms of $\hat{\omega}$, $E_{\text{rms}}(\hat{\beta})$ and $\widehat{\Phi}_f$. Comparisons of the results show that the accuracy of $\hat{\omega}$, $\hat{\beta}_2$ and $\widehat{\Phi}_f$ decreases, as the σ increases, for all values of ω considered. If we plot the curves of $\widehat{\Phi}_f$ versus θ_0 for $\sigma = 0.0, 0.001, 0.01$, the comparison of the curves reveals that the dependence of $\widehat{\Phi}_f$ on σ is relatively small. Table 2 also shows that the accuracy of the estimated results decreases with the increase of ω.

Fig. 10 shows the estimated results of β for the two-dimensional cases with $\Phi = \Phi_b$, $\beta = \beta_3$, $\omega = \omega_2$ and $\sigma = 0.001$, 0.01, 0.05. The estimated results of the β even obtained from measurement data with $\sigma = 0.05$ are still

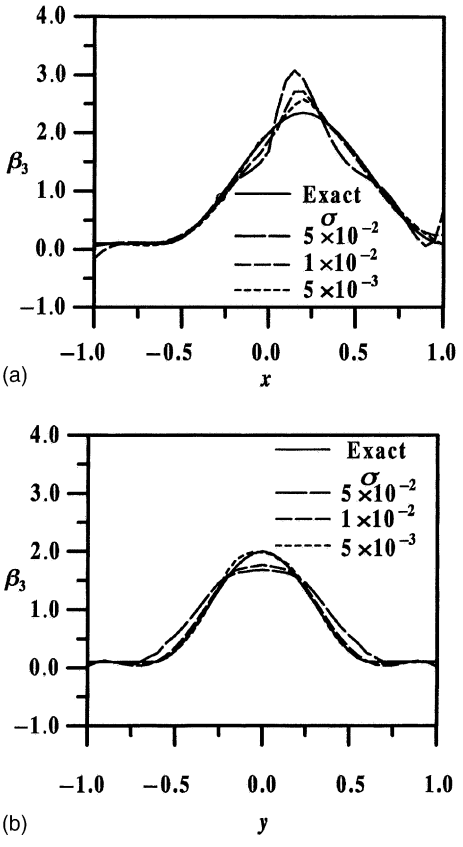

Fig. 10. Effects of the measurement error for the case with $\beta = \beta_3$, $\Phi = \Phi_b$ and $\omega = 0.5$: distributions of the β along (a) the x-axis, (b) y-axis.

acceptable. The discrepancy between the distributions of the β_3 and $\hat{\beta}_3$ along the x- and the y-axis increases as σ increases, as shown in Fig. 10(a) and (b), respectively. The dependence of $\hat{\omega}$ and $\widehat{\Phi}_f$ on σ is similar to that found for the one-dimensional cases shown in Table 2.

Finally, we consider the reconstruction of the extinction coefficient and the albedo for a finite cylindrical medium with $\Phi = 1$, $\beta = \beta_4$, $\omega = 0.5$, and unity optical thickness in the z-direction. In this three-dimensional case, we divide the domain into $N_r \times N_\psi \times N_z = 10 \times 24 \times 10$ cells and solve the radiative transfer equation along $N_{\psi_x} \times M_\theta = 12 \times 5$ discrete ordinates. We adopted $\widehat{M}_\beta = 5$, $\widehat{N}_\beta = 3$ and $\widehat{L}_\beta = 3$ to reconstruct the distribution of the extinction coefficient and the albedo. The value of the estimated albedo is 0.492. Fig. 11(a) and (b) show the distributions of the extinction coefficient over the x-axis on the z cross-sections, $z = 0.5$ and 0.95, respectively. It is seen that the discrepancies among the exact one, the estimated one and the estimated result obtained by the two-dimensional scheme are small, especially on the central cross section ($z = 0.5$). The comparison reveals that the two-dimensional scheme

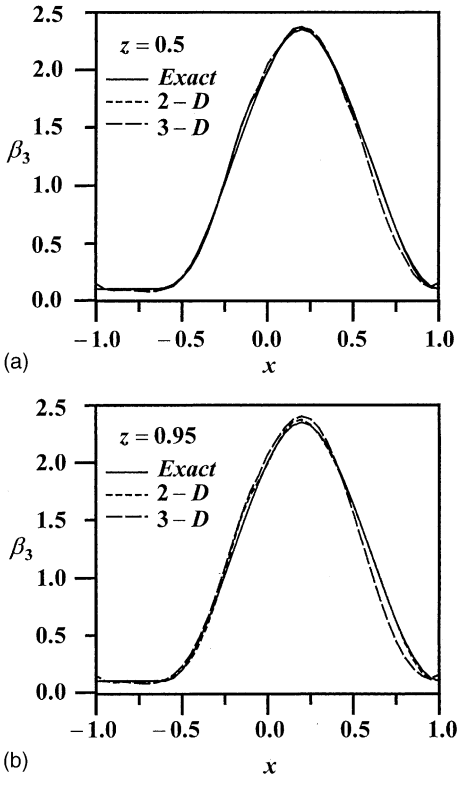

Fig. 11. Distributions of the exact and estimated β's for the case with $\beta = \beta_3$, $\Phi = 1.0$ and $\omega = 0.5$: distributions of the β along (a) the x-axis, (b) y-axis.

using less computer source can replace the three-dimensional scheme, when the distribution of the extinction coefficient is uniform in the z-direction.

4. Conclusions

This study developed the schemes for the simultaneous estimation of distribution of the extinction coefficient, the scattering albedo and the phase function under a completely scattering model. The schemes can reconstruct accurate enough results for most of the cases considered. The results show that the case with a non-smooth distribution of the extinction coefficient needs more cells and more terms of the expansion of the estimated extinction coefficient to obtain accurate enough estimated results. The accuracy of the estimated results decreases with the increase of the scattering albedo. For an optically thin case, we need more discrete ordinates to generate accurate enough estimated results. The number of the expansion coefficients of the phase function does not have strong influence on recovering relevant parameters. The estimated results obtained from the measurement data with moderate errors are still acceptable. This scheme can be extended to three-dimensional cases readily.

Acknowledgements

This work is supported by the National Science Council of the Republic of China on Taiwan through Grant NSC 90-2212-E006-166.

References

[1] Y. Yamada, Light-tissue interaction and optical imaging in biomedicine, in: C.L. Tien (Ed.), Annual Review of Heat Transfer, Begell House, New York, Chapter 1, vol. 6, 1995.
[2] S.R. Arridge, Optical tomography in medical imaging, Inverse Prob. 15 (1999) R41–R93.
[3] B.J. Hughey, D.A. Santavicca, A comparison of techniques for reconstructing axisymmetric reacting flow fields from absorption measurements, Combust. Sci. Technol. 29 (1982) 167–190.
[4] M. Ravichandran, F.C. Gouldin, Determination of temperature and concentration profiles using (a limited number of) absorption measurements, Combust. Sci. Technol. 45 (1986) 47–64.
[5] B.M. Agarwal, M.P. Mengüc, Forward and inverse analysis of single and multiple scattering of collimated radiation in an axisymmetric system, Int. J. Heat Mass Transfer 34 (1991) 633–647.
[6] E.D. Torniainen, F.C. Gouldin, Tomographic reconstruction of 2-D absorption coefficient distributions from a limited set of infrared absorption data, Combust. Sci. Technol. 131 (1998) 85–105.
[7] W.W. Yuen, A. Ma, I.C. Hsu, G.R. Cunnington Jr., Determination of optical properties by two-dimensional scattering, J. Thermophys. 6 (1992) 182–185.
[8] V.V. Alpatov, Y.A. Romanovsky, Methods of optical tomography for remote sensing of the atmosphere and near-earth space, Adv. Space Res. 21 (1998) 1437–1440.
[9] C.J. Dasch, One-dimensional tomography: a comparison of Abel, onion-peeling, and filtered backprojection methods, Appl. Optics 31 (1992) 1146–1152.
[10] M.P. Mengüc, P. Dutta, Scattering tomography and its application to sooting diffusion flames, J. Heat Transfer; Trans. ASME 116 (1994) 144–151.
[11] E. Okada, M. Firbank, M. Schweiger, S.R. Arridge, M.C. Cope, D.T. Delpy, Theoretical and experimental investigation of near-infrared light propagation in a model of the adult head, Appl. Optics 36 (1997) 21–31.
[12] N.J. McCormick, Inverse radiative transfer problems: a review, Nucl. Sci. Eng. 112 (1992) 185–198.
[13] R. Aronson, R.L. Barbour, J. Lubowsky, H. Graber, Application of transport theory to infra-red medical imaging, in: W. Greenberg, J. Polewczak (Eds.), Modern Mathematical Methods in Transport Theory, Birkhäuser Verlag, Basel, 1991, pp. 64–75.
[14] J.H. Chang, H.L. Graber, R.L. Barbour, R. Aronson, Recovery of optical cross-section perturbations in

dense-scattering media by transport-theory-based imaging operators and steady-state simulated data, Appl. Optics 35 (1996) 3963–3972.

[15] A.D. Klose, A.H. Hielscher, Iterative reconstruction scheme for optical tomography based on the equation of radiative transfer, Med. Phys. 26 (1999) 1698–1707.

[16] A.D. Klose, A.H. Hielscher, Optical tomography using the time-independent equation of radiative transfer—part II: inverse model, J. Quant. Spectrosc. Radiat. Transfer 72 (2002) 714–732.

[17] B.-T. Liou, C.-Y. Wu, Ray effecting the discrete ordinate solution for surface radiation exchange, Heat Mass Transfer 32 (1997) 271–275.

[18] M.A. Ramankutty, A.L. Crosbie, Modified discrete-ordinates solution of radiative transfer in three dimensional rectangular enclosures, J. Quant. Spectrosc. Radiat. Transfer 60 (1998) 103–134.

[19] S.-C. Hsu, C.-Y. Wu, N.-R. Ou, Azimuthally dependent radiative transfer in a nonhomogeneous cylindrical medium, Radiat. Phys. Chem. 53 (1998) 107–113.

[20] D.W. Marquardt, An algorithm for least-squares estimation of nonlinear parameters, J. Soc. Indust. Appl. Math. 11 (1963) 431–441.

[21] H.P. William, A.T. Saul, T.V. William, P.F. Brain, in: Numerical Recipes, Chapter 15, second ed., Cambridge University Press, New York, 1992.